Desalination and Water Treatment
www.deswater.com
doi: 10.5004/dwt.2022.28158

253 (2022) 113–121
March

Effect of divalent manganese ions on the roxarsone removal efficiency from aqueous solution with iron oxide

Wenjuan Shen[a,*], Menghan Xiao[a], Zixin Yao[a], Zhan Liu[a], Qi Feng[a], Xu Zhang[b], Wenqing Wang[a], Jianfen Li[a,*], Xing Peng[b,*], Fengjiao Quan[a], Menghua Cao[c], Shunxi Zhang[a], Zhenhua Qin[a]

[a]*Department of Chemistry and Environment Engineering, Wuhan Polytechnic University, Wuhan, 430023, China, emails: wenjuan_shen@whpu.edu.cn (W. Shen), whpulijfen@126.com (J. Li)*
[b]*Key Laboratory of Pesticide & Chemical Biology of Ministry of Education, Institute of Environmental & Applied Chemistry, Central China Normal University, Wuhan 430079, China, email: pengxing185@163.com (X. Peng)*
[c]*College of Resources and Environment, Huazhong Agricultural University, Wuhan 430070, China*

Received 12 August 2021; Accepted 6 January 2022

ABSTRACT

In this study, the effect of Mn(II) on the roxarsone (ROX) removal efficiency by iron oxide was systematically investigated. ROX removed by iron oxide obeyed pseudo-second-order non-linear kinetic model with the addition of Mn(II), and the removal rate constant normalized by specific surface area was calculated to be 4.5×10^{-3} g m^{-2} h^{-1}, which was 4.8 times than that in the absence of Mn(II). Based on a series of experimental and characterization results, we found that Mn(II) could not be oxidized to Mn(III) in the presence of iron oxide, and the enhanced ROX removal process was attributed to the promoted ROX adsorption process. Further zeta potential results suggested that the addition of Mn(II) increased the isoelectric point of iron oxide from 5.3 to 7.5, which provided positive adsorption site favoring adsorption process of the negative charged arsenic functional group in ROX. This investigation provided fundamental understanding for the effect of Mn(II) on the removal efficiency of ROX by iron oxide.

Keywords: Divalent manganese ions; Roxarsone; Iron oxide; Removal mechanism

1. Introduction

Aromatic organoarsenicals, such as roxarsone (3-nitro-4-hydroxyphenylarsonic acid, ROX) and p-arsanilic acid (4-aminophenylarsonic, *p*-ASA), used as feed additive, has been widely applied for coccidiosis control and feed conversion promotion for decades [1]. However, most of these organoarsenic compounds little metabolized in the poultry or swine bodies, and almost excreted without transformation through manure and urine, resulting in the high level of organoarsenic compounds in the surface soils near swine farms [2,3]. Although the toxicity of organic arsenic is less than that of inorganic arsenic, long-term usage could inhibit activity of enzyme, and lead to the collapse of animal tissues and organs [4]. Meanwhile, the high solubility of ROX in aqueous solution resulted in its high leakage risk from manures, which might lead to water pollution by organic arsenic [5]. Moreover, these organoarsenic compounds introduced into the natural environment via animal manure and urine could be converted into dimethylarsinic

* Corresponding authors.

acid (DMA) and inorganic arsenic (iAs) with much higher toxicity and mobility through biotic or abiotic processes [2,6–9]. Therefore, understanding the migration and transformation behavior of organoarsenic compounds in natural environment is of great significance.

The previous studies revealed that metal (oxyhydr) oxides, especially iron (oxyhydr)oxides, an important component in soil and sediments, played a vital role in adsorption of plentiful arsenic species, including inorganic and organic arsenic [10–15]. For example, Xie and Cheng [10] revealed that arsonic acid group of *p*-ASA and ROX could form inner-sphere complexes on the surface of iron (oxyhydr)oxides and γ-MnO_2, and those organoarsenic compounds adsorption processes were promoted by Fe^{3+} capable to form hydrous ferric oxide precipitation with high affinity to arsenicals, but barely affected by co-existed cations (i.e., Ca^{2+}, Cu^{2+}, Mg^{2+}, and Zn^{2+}). Zhang et al. [16] revealed that molecular configurations of organic arsenics adsorbed on hematite depended on exposed facet of hematite. Chen et al. [17] found that the similar adsorption trends of ROX and *p*-ASA with goethite and aluminum oxide could be found, while the surface adsorption site of Al_2O_3 was approximately 3 times lower than that for FeOOH. Based on these studies, iron (hydro)oxide was a kind of reactive minerals which could adsorb organic arsenics. Considering that iron (oxyhydr)oxides often coexisted with divalent manganese ions (Mn(II)) originated from the reduction of Mn mineral in many redox-active environments, and iron (oxyhydr)oxides could catalyze the oxidation of Mn(II) by oxygen to generate minerals with Mn(III), including Mn_3O_4, β-MnOOH, and γ-MnOOH, which could oxidize organic matter [18–21], it was speculated that adsorption and oxidation might be involved during the organic arsenic removal process by iron (oxyhydr)oxides in the presence of Mn(II).

To better understand the interaction among (oxyhydr) oxides, organoarsenic, and Mn(II) in environment, hematite and ROX were selected as model (oxyhydr)oxides and organoarsenic to investigate the interaction mechanism between (oxyhydr)oxides and organic arsenic with the addition of divalent manganese ions in this study. By comparing the ROX concentration in solution and on the surface of hematite, the ratio of adsorption and oxidation behavior of ROX could be obtained. Besides, attenuated total reflectance-Fourier transform infrared (ATR-FTIR) spectroscopy was utilized to reveal the difference in adsorption configuration with or without the addition of Mn(II), and X-ray photoelectron spectroscopy (XPS) was employed to analyze the variation of elements valence. This study provided deep understanding for the process and mechanism of ROX migration and transformation in environment.

2. Materials and methods

2.1. Chemicals and materials

ROX (4-hydroxy-3-nitrophenylarsonic, >98.0%) was purchased from TCI Chemicals (Shanghai, China), Fe_2O_3 (99.7%) was obtained from Aladdin Reagent (Shanghai) Co., Ltd., China without further purification, manganese(II) chloride tetrahydrate, sodium hydroxide, and other reagents were of analytical grade and provided by Sinopharm Chemical Reagent Co., Ltd., China. All reagents were used as received without further treatment. Deionized water was used throughout the experiments.

2.2. ROX removal with hematite and Mn(II)

In a typical process, 0.05 g of Fe_2O_3 powder was added into a 100 mL conical flask containing 50 mL of ROX (20 mg L^{-1}) solution in the presence or absence of 0.5 mmol L^{-1} Mn(II) without pH adjustment unless specified statement, and 10 mmol L^{-1} NaCl solution was used as the background electrolyte. The reaction vessel was placed on a gyrotron oscillator open to air at 25°C with fixed oscillation rate of 220 rpm, and samples were collected at regular time interval by syringe-filtered using 0.22 μm polytetrafluoroethylene (PTFE) membrane for the subsequent ROX concentration analysis.

2.3. Analytical methods

The concentration of ROX was analyzed by a high-performance liquid chromatography (HPLC, 1260 Infinity, Agilent) equipped with an Agilent reversed-phase column (ZORBAX SB-C18, 150 mm × 4.6 mm, 5 μm). The mobile phase consists of 70% phosphoric acid (0.05 mmol L^{-1}) and formic acid (0.1%), 30% methanol at the flow rate of 1.0 mL min^{-1}. The absorption wavelength of UV detector was fixed at 260 nm. In order to determine the amount of adsorbed ROX on the surface of Fe_2O_3 with the addition of Mn(II) and residual ROX in solution during the removal process, concentrated hydrochloric acid was used to dissolve Fe_2O_3 powder, and the final solution was analyzed by HPLC. For the detail procedure, 5 mg Fe_2O_3 particles and 0.05 mmol L^{-1} Mn(II) was added into 5 mL ROX (20 mg L^{-1}) solution. Subsequently, 5 mL of 66.7% hydrochloric acid was added into the suspension solution containing Fe_2O_3 particles and ROX. To accelerate the dissolution process, the suspension was stirred with fixed rate about 1 min at 70°C. And then, the dissolved suspension solution was filtered using 0.22 μm PTFE membrane, and the ROX concentration was analyzed by HPLC. Formaldoxime colorimetric method and electron spin resonance spectrum (ESR) were used to measure the concentration of dissolved Mn(II) [22]. As the initial Mn(II) concentration in reaction solution exceed detection limit by formaldoxime colorimetric method, samples were diluted by 100 times before tested.

2.4. Characterization

The morphology and crystal structures of Fe_2O_3 before and after reaction were recorded by scanning electron microscopy (SEM, SU8010) and X-ray diffraction (XRD, Shimadzu XRD-7000X) equipped with Cu Kα radiation. The specific surface area of Fe_2O_3 was analyzed via N_2 adsorption and desorption curves (Micromeritics 2460). The elements valence on the surface of Fe_2O_3 were measured by XPS (Thermo Scientific K-Alpha). The zeta potential of hematite in the absence or presence of Mn(II) with pH values ranged from 3 to 10 was determined by DTS 1070 Zetasizer and nanoparticle size analyzer (Malvern Panalytical, Malvern, UK) using 10 mmol L^{-1} NaCl as the background electrolyte. ATR-FTIR spectra were collected by FTIR spectrometer (Nicolet Is50, Thermo) equipped with a diamond internal reflection unit and a mercury-cadmium-telluride (MCT) detector. The detail analysis information was the same as literatures [16].

3. Results and discussion

3.1. Removal of ROX by Fe_2O_3 in the presence and absence of Mn(II)

To evaluate the effect of Mn(II) on ROX removal by Fe_2O_3, we monitored the ROX concentration variation with or without the addition of Mn(II). As presented in Fig. 1a, the percentages of ROX removal with Fe_2O_3 within 96 h in the absence and presence of Mn(II) were 67.16% and 88.38%, respectively, suggesting that Mn(II) enhanced the ROX removal efficiency significantly. As the control, Mn(II) alone could not remove any ROX. In addition, the ROX removal curves with or without the addition of Mn(II) fitted well with the pseudo-second-order non-linear kinetic model of high correlation coefficients ($R^2 > 0.999$) (Fig. 1b). Considering that the specific surface area of Fe_2O_3 was 131 $m^2\ g^{-1}$, the apparent ROX removal rate constant of Fe_2O_3 with the addition of Mn(II) was calculated to be 4.5×10^{-3} g $m^{-2}\ h^{-1}$, which was 4.8 times than that without the addition of Mn(II). Moreover, to further confirm the kinetic model for ROX removal process, zero-order and pseudo-first-order kinetics fitting were further analyzed (Figs. 1c and d), and the related parameters of coefficient of determination (R^2), chi-square, and sum of the squares of the errors (SSE) are summarized in Table 1. It was found that the values of R^2 for zero-order and pseudo-first-order kinetic fitting curves in the presence and absence of Mn(II) were only 0.692, 0.736, 0.570, and 0.767, respectively, suggesting that the zero-order and pseudo-first-order kinetic equations were not suitable for the ROX removal process. Meanwhile, values for the squares of errors and the chi-square test with the pseudo-second-order kinetic fitting were reasonable [23]. Therefore, it could be concluded that the ROX removal process obeyed pseudo-second-order kinetic model.

Subsequently, to determine the maximum immobilization capacity of Fe_2O_3 with or without the addition of Mn(II), the sorption isotherms based on the different initial ROX concentrations ranged from 20 to 250 mg L^{-1} were investigated. It was found that the presence of Mn(II) indeed promoted the ROX removal percentage, and the ROX removal percentage decreased from 88.46% to 30.80% with the increase of ROX concentration (Figs. 2a and b). Moreover, Langmuir isotherm model and Freundlich isotherm model were utilized to analyze the ROX adsorption equilibrium. The linear formula of Langmuir equation could be written as Eq. (1) [17].

$$\frac{C_e}{q_e} = \frac{1}{q_m K_L} + \frac{C_e}{q_m} \tag{1}$$

where C_e (mg L^{-1}) is the equilibrium concentration of ROX, q_e (mg g^{-1}) is the ROX equilibrium adsorption amount, q_m (mg g^{-1}) and K_L (L mg^{-1}) were the maximum adsorption capacity and the equilibrium constant, respectively.

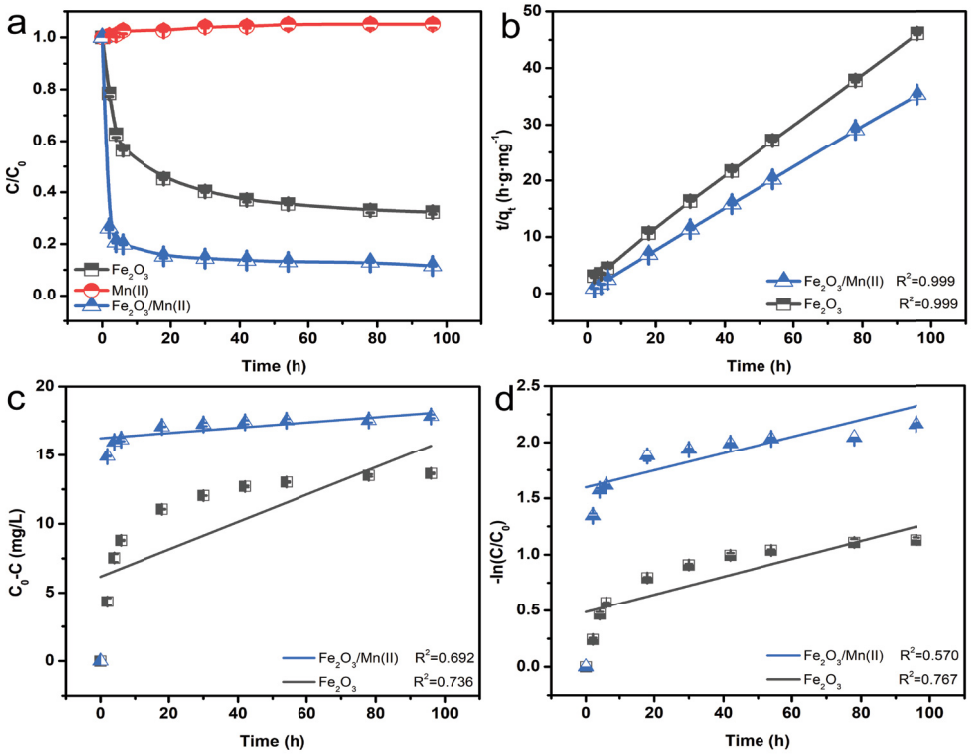

Fig. 1. (a) Time profiles of ROX removal with Fe_2O_3 in the presence and absence of Mn(II); (b) pseudo-second-order, (c) zero-order, and (d) pseudo-second-order kinetics fitting curves of ROX removal in the Fe_2O_3 and Fe_2O_3/Mn(II) system. The initial concentrations of Fe_2O_3, Mn(II) and ROX were 1.0 g L^{-1}, 0.5 mmol L^{-1} and 20.0 mg L^{-1}, respectively. 10 mmol L^{-1} NaCl was used as the background electrolyte. Error bars represent ± one standard deviation derived from triplicate experiments.

Table 1
Related parameters of different kinetics fitting for ROX removal process

Kinetics model	System	Coefficient of determination (R^2)	Sum of the squares of the errors (SSE)	Chi-square measure
Zero-order	Fe_2O_3/Mn(II)	0.692	0.123	0.0175
	Fe_2O_3	0.736	2.536	0.362
Pseudo-first-order	Fe_2O_3/Mn(II)	0.570	0.00297	0.000424
	Fe_2O_3	0.767	0.00267	0.000382
Pseudo-second-order	Fe_2O_3/Mn(II)	0.999	0.02394	0.00342
	Fe_2O_3	0.999	0.05355	0.00765

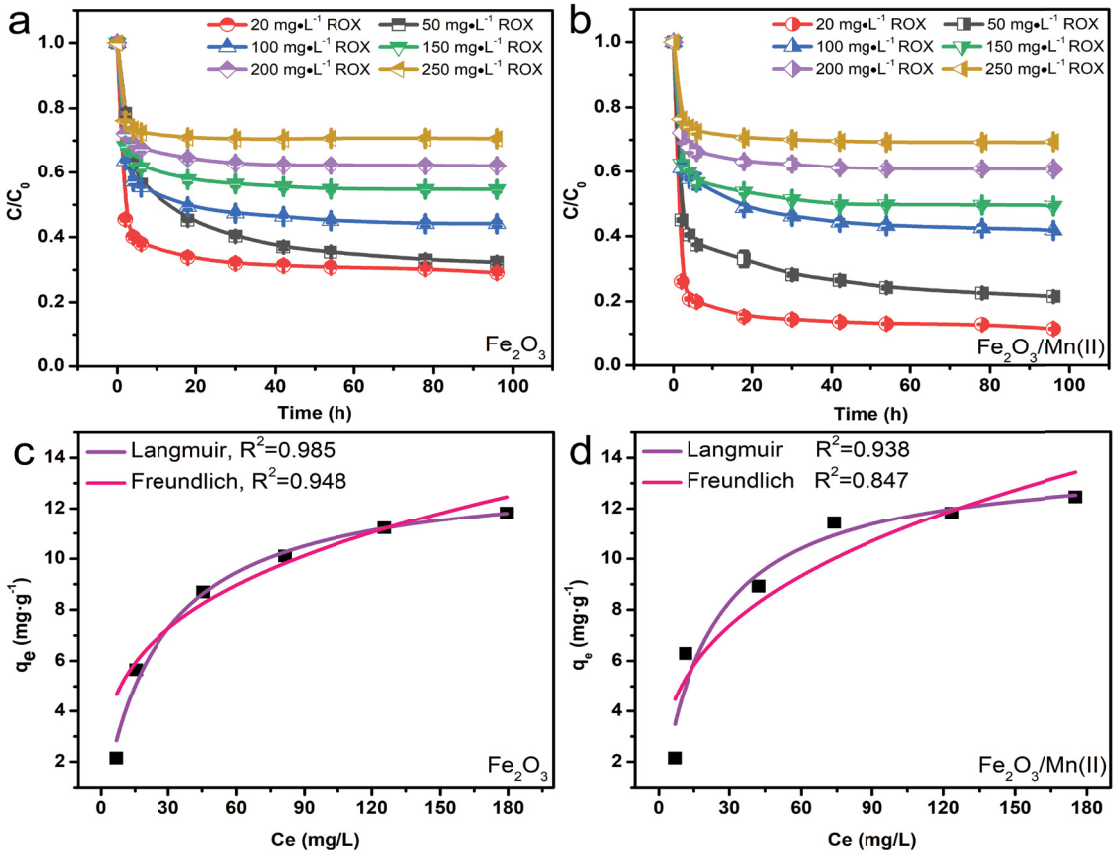

Fig. 2. Time profile of ROX adsorption with (a) Fe_2O_3, (b) Fe_2O_3 and Mn(II), (c) Langmuir plot and Freundlich plot for the adsorption of ROX on Fe_2O_3 and (d) Langmuir plot and Freundlich plot for the adsorption of ROX on Fe_2O_3/Mn(II). The dosage of Fe_2O_3 was 1.0 g L^{-1}. The initial pH was 4.3 without any adjustment. The initial ROX concentrations (bottom to top) range from 20 to 250 mg L^{-1}. 10 mmol L^{-1} NaCl was used as the background electrolyte. Error bars represent ± one standard deviation derived from triplicate experiments.

The linear form of the Freundlich model could be represented as Eq. (2) [24].

$$\ln q_e = \ln K_F + \frac{1}{n}\ln C_e \tag{2}$$

where K_F (mg^{1-n} g^{-1} L^{-n}) was attributed to adsorption capacity, and $1/n$ was Freundlich constants related to adsorption intensity. The related equilibrium adsorption isotherm fitting parameters are summarized in Table 2. We found that ROX removal process fitted better with the Langmuir model than the Freundlich model (Figs. 2c and d), indicating that monolayer coverage was preferred for ROX adsorption on Fe_2O_3.

3.2. Oxidation and adsorption ratio of removed ROX

According to the previous studies, Mn(II) adsorbed on Fe_2O_3 surface could be oxidized by molecular oxygen (O_2)

to form Mn(III, IV) oxides and oxyhydroxides [19,21], and the formed Mn minerals could oxidize the organic matter in turn. Therefore, the enhanced ROX removal efficiency with the addition of Mn(II) might be attributed to the promoted ROX oxidation process by the manganese minerals in this study. Meanwhile, as the toxicity of inorganic arsenic was much higher than that of organic arsenics compounds, and the oxidation of ROX usually resulted in the cleavage of C-As bond, leading to the generation of inorganic arsenic, such as arsenite and arsenate [14], therefore, it is of great significance to reveal the ratio of oxidized ROX to adsorbed ROX in the presence and absence of Mn(II). Since molecular oxygen was involved in the Mn(II) oxidation process, the ROX removal rate would be decreased when dissolved oxygen (DO) was eliminated from aqueous solution if both oxidation and adsorption processes involved in the Fe_2O_3/Mn(II) system. Therefore, we compared the ROX removal performance at Air and Ar atmosphere. As presented in Fig. 3a, there was no significant difference between the Fe_2O_3/Mn(II)/Air and Fe_2O_3/Mn(II)/Ar system in ROX removal curves, indicating that the oxidation mechanism was excluded during the ROX removal process in the Fe_2O_3/Mn(II)/Air system. In addition, as the oxidation degradation of ROX would result in the decrease of ROX concentration in aqueous solution and on Fe_2O_3 surface, we therefore measured unreacted ROX in aqueous solution and ROX adsorbed on the iron oxide surface by dissolving the Fe_2O_3 with concentrated hydrochloric acid, and then analyzed the dissolved ROX concentration using HPLC. As shown in Fig. 3b, the total ROX concentration kept stable around 20 mg L^{-1}, further suggesting that ROX could not be degraded in the Fe_2O_3/Mn(II)/Air system.

Meanwhile, as organic matter oxidation process was caused by the Mn(II) oxidation products adsorbed on Fe_2O_3 surface, and the Mn(II) oxidation process was accompanied with the decreased Mn(II) concentration in solution, we further monitored the Mn(II) concentration variation in the Fe_2O_3/Mn(II)/Air system by formaldoxime colorimetric method and electron spin resonance spectrum (ESR). It was found that Mn(II) concentration after diluted by 100 times kept stable around 0.34 mg L^{-1} (Fig. 4a), indicating that neither adsorption of Mn(II) on Fe_2O_3 surface nor the oxidation of Mn(II) catalyzed by Fe_2O_3 could occur in this study. This conclusion could be further confirmed by ESR results as the signal intensity attributed to Mn(II) did not decreased with time (Fig. 4b). To further verify that Mn(II) did not transform into Mn(III), pyrophosphate (PP) was added into the Fe_2O_3/Mn(II) system since PP could form complex with Mn(III), which could be monitored by UV-Vis spectra [25]. However, no apparent peak around 258 nm assigned to the complex of PP and Mn(III) was found, indicating that Fe_2O_3 could not oxidize Mn(II) into Mn(III) (Fig. 4c).

3.3. Characterizations of Fe_2O_3 before and after ROX removal reaction

To determine whether the morphologies and crystalline structures of Fe_2O_3 varied after ROX removal, SEM images and XRD patterns were collected. As presented in Figs. 5a and b, Fe_2O_3 before and after ROX removal with

Table 2
Equilibrium adsorption isotherm fitting parameters

Entry	Langmuir isotherm			Freundlich isotherm		
	K_L (L mg^{-1})	q_m (mg g^{-1})	R^2	K_F (mg^{1-n} g^{-1} L^{-n})	n	R^2
Fe_2O_3/Mn(II)	0.049	13.96	0.9374	2.33	2.9516	0.8469
Fe_2O_3	0.039	13.49	0.9854	2.62	3.3257	0.9484

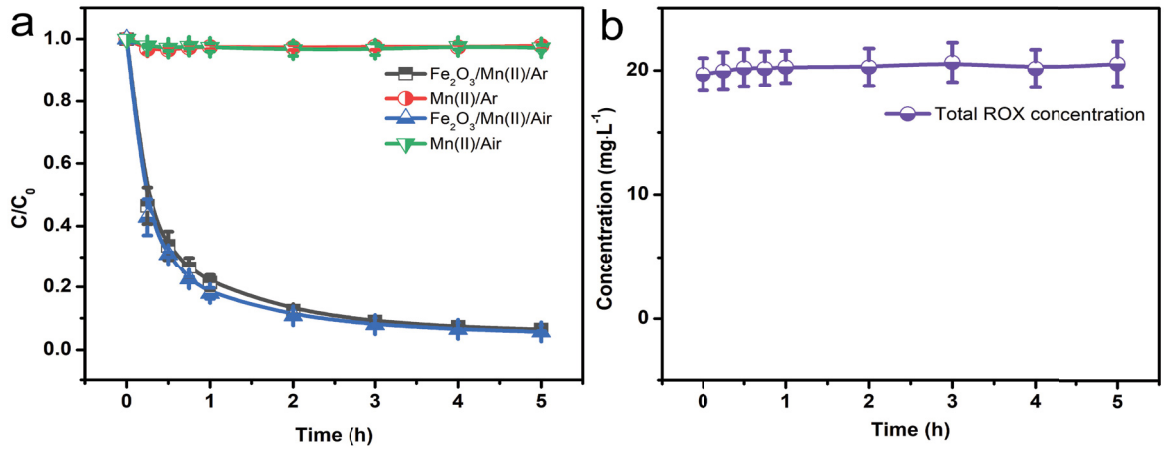

Fig. 3. (a) Effect of solution dissolved oxygen on ROX adsorption by Fe_2O_3 and (b) concentrations of ROX absorbed on Fe_2O_3 surface and residual in solution vs. time. The initial concentrations of Fe_2O_3, Mn(II) and ROX were 1.0 g L^{-1}, 2.0 mmol L^{-1} and 20.0 mg L^{-1}, respectively. Error bars represent ± one standard deviation derived from triplicate experiments.

the addition of Mn(II) showed rod-like structure around 200–500 nm in length. Peaks of samples before and after reaction matched well with the JCPDF file No. 99-0060 (Fig. 5c). Subsequently, to further confirm that Mn(II) could not be oxidized by Fe_2O_3 or be adsorbed on the surface of Fe_2O_3, we used XPS to characterize the surface elements composition and valence of Fe_2O_3 before and after reaction. It was found that there was no peaks attributed to Mn element in the full-range and high-resolution XPS spectra of Fe_2O_3 with the addition of Mn(II) (Figs. 6a and b), suggesting that the oxidation and adsorption process of Mn(II) could not occur on the surface of Fe_2O_3. In contrast, binding energy around 45.2 eV corresponding to As 3d was found on surface of Fe_2O_3 (Fig. 6c) with or without the addition of Mn(II), further indicating the adsorption of ROX on Fe_2O_3 [26].

According to the present studies, organic arsenics compounds adsorbed on iron oxide with different exposed facet could form different molecular configurations, resulting in different *p*-ASA adsorption efficiency [16]. To determine whether the different ROX adsorption efficiency of Fe_2O_3 with the addition of Mn(II) was caused by the different ROX adsorption configurations, representative ATR-FTIR spectra of ROX were monitored in different ROX concentrations. As shown in Fig. 7a, it was found that peaks around 1,325

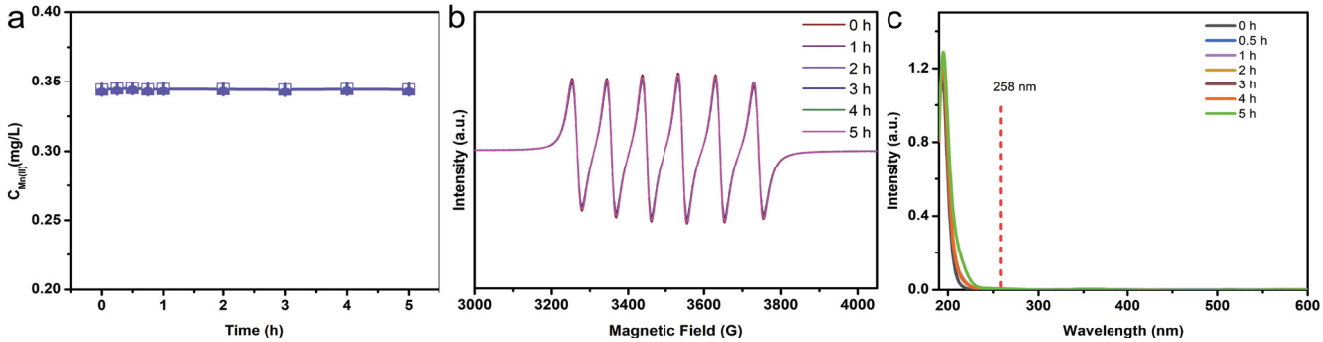

Fig. 4. (a) Mn(II) concentration variation in the presence of Fe_2O_3 and ROX monitored by UV-Vis spectrum and (b) Mn(II) concentration variation monitored by electron spin resonance spectrum; (c) UV-Vis spectrum reaction solution in the Fe_2O_3/Mn(II) system with the addition of pyrophosphate (PP). The initial concentrations of Fe_2O_3, Mn(II), ROX, and PP were 1.0 g L^{-1}, 2.0 mmol L^{-1}, 20.0 mg L^{-1} and 50 mmol L^{-1}, respectively. Error bars represent ± one standard deviation derived from triplicate experiments.

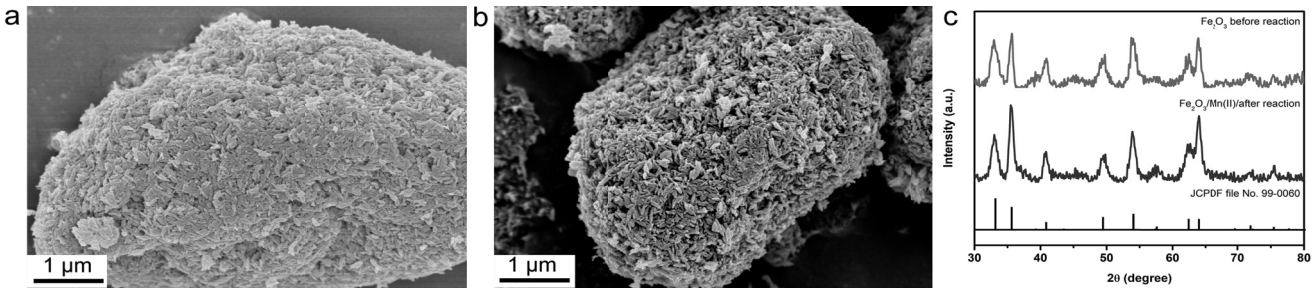

Fig. 5. SEM images of (a) Fe_2O_3 before reaction, (b) Fe_2O_3 after reaction in the presence of Mn(II). (c) XRD patterns of Fe_2O_3 before and after reaction in the presence of Mn(II).

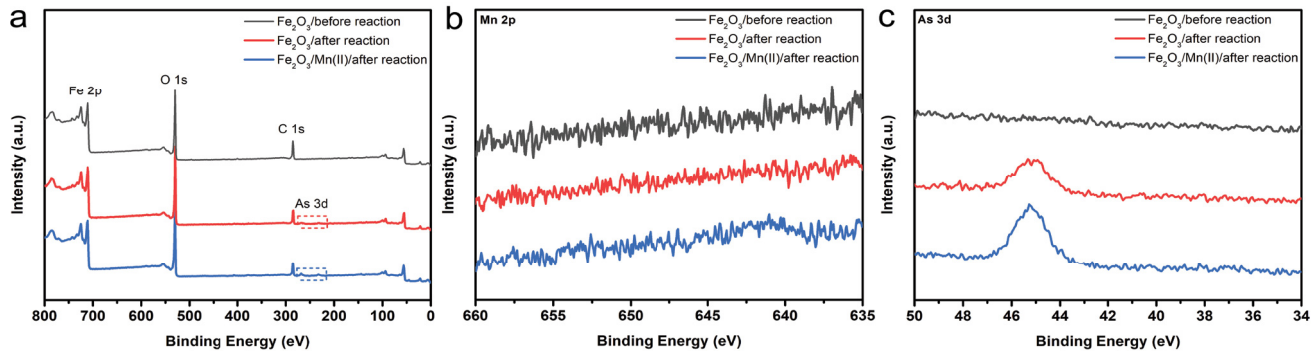

Fig. 6. (a) Full-range XPS spectra of Fe_2O_3 powder in the presence and absence of Mn(II) before and after ROX adsorption. High-resolution XPS spectra of Fe_2O_3 powder before and after ROX adsorption for (b) Mn 2p, and (c) As 3d.

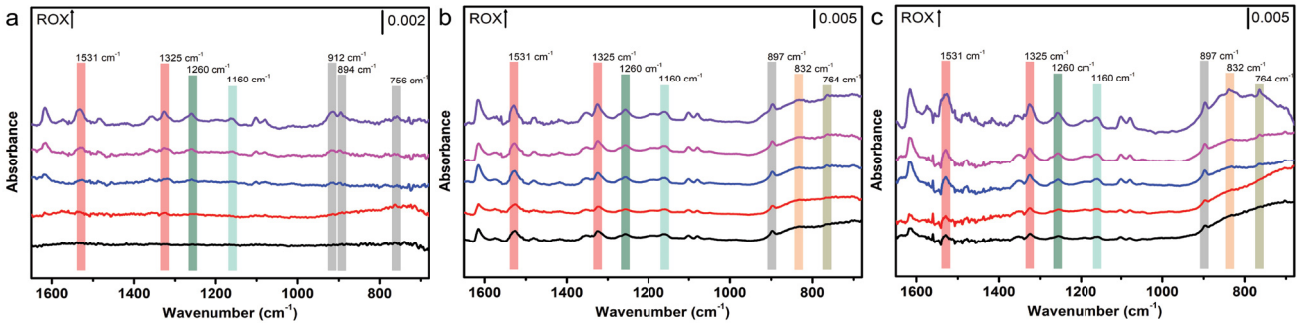

Fig. 7. ATR-FTIR absorption spectra of (a) ROX, (b) Fe_2O_3/ROX, and (c) Fe_2O_3/Mn(II)/ROX. The ROX concentrations (bottom to top) were 1.0, 3.0, 5.0, 10.0, and 20.0 g L^{-1}, respectively.

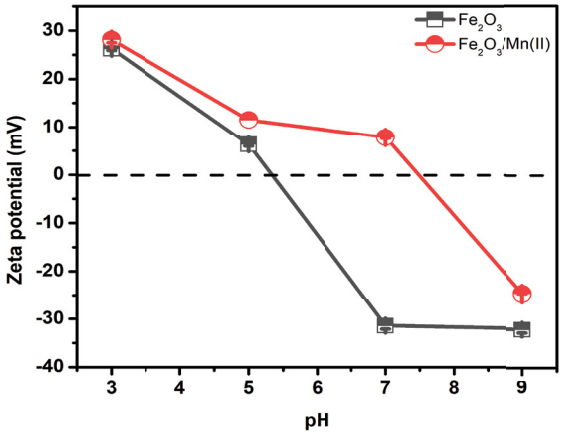

Fig. 8. Zeta potential distribution of Fe_2O_3 in the presence or absence of Mn(II) vs. pH values. Error bars represent ± one standard deviation derived from triplicate experiments.

and 1,531 cm^{-1} were ascribed to symmetrical and asymmetrical stretching vibration of $-NO_2$, respectively [27]. Meanwhile, peaks associated with the vibration of C–N and C–As arose at 1,260 and 1,160 cm^{-1} [28]. Moreover, the typical As–O bond originated from the $-AsO(OH)_2$ of ROX were located at 912, 894, and 756 cm^{-1} [24]. Subsequently, we compared the ATR-FTIR spectra of ROX using Fe_2O_3 as adsorbent with or without the addition of Mn(II) (Figs. 7b and c). It was found that the addition of divalent manganese ions did not affect the ROX adsorption configuration since ATR-FTIR spectra of the ROX adsorption by Fe_2O_3 did not change significantly with the addition of Mn(II). Component observed at 897 cm^{-1} indicated the presence of $-AsO_3H^-$, and intense peak at 832 cm^{-1} could be attributed to H-bonded complex [29]. Meanwhile, component <800 cm^{-1} was assigned to inner-sphere complex As–O–Fe [29]. Based on the ATR-FTIR spectra results, it could be concluded that both H-bond complexes and inner-sphere complexes could be formed during the ROX adsorption process using Fe_2O_3 as adsorbents.

3.4. Zeta potential of Fe_2O_3 mineral in the presence and absence of Mn(II)

Since hydroxyl group on the surface of iron oxide could form variable surface charge through protonation and deprotonation processes, and the ligand exchange with surface $-OH_2^+$, rather than surface OH^- groups, figured prominently in arsenate adsorption under acidic conditions, it was reasonable to speculate that Mn(II) might enhanced the ROX removal performance via changed the surface charge distribution. To check whether the promoted ROX removal was attributed to the varied surface charge after the Mn(II) addition, the zeta potential distribution of iron oxide among various pH values were monitored. As presented in Fig. 8, the addition of Mn(II) increased the isoelectric point of Fe_2O_3 from 5.3 to 7.5. Since the pK_a value of ROX was 3.45, 5.95, and 9.15 [30–32], ROX in solution would in the form of organoarsenic anions (i.e., $H_2AsO_3R^-$ and $HAsO_3R^{2-}$) when the pH value was 4.3. Therefore, the more positively charged iron oxide with the addition of Mn(II) favored the adsorption process of organoarsenic anions.

3.5. Cyclic stability of ROX removal by iron(III) oxide and Mn(II)

Based on the above experiment results, it could be concluded that Mn(II) improved the ROX adsorption process by Fe_2O_3. To further confirm this conclusion, 0.1 mol L^{-1} NaOH aqueous solution was utilized to elute the adsorbed ROX on the surface of Fe_2O_3, and then repeated the ROX adsorption experiments with the addition of Mn(II). The results showed that after five runs there was no significant decrease in ROX removal efficiency (Fig. 9), further suggesting that adsorption process was the dominant removal mechanism for ROX.

3.6. ROX removal by iron(III) oxide in real wastewater samples

To investigate the ROX removal efficiency by Fe_2O_3 with or without Mn(II) in real wastewater samples, ROX was added into the swine wastewater obtained from Wuhan Xinnongyuan Farm. As shown in Fig. 10, the removal percentage of ROX with Fe_2O_3 within 300 min in the presence of Mn(II) was 91.96%, which was 6.23 times that in the absence of Mn(II) (14.77%). The results show that Fe_2O_3/Mn(II) system was also applicable for ROX removal in aquaculture wastewater.

4. Conclusions

In this study, the mechanism of ROX removal by Fe_2O_3 with or without the addition of Mn(II) was reported.

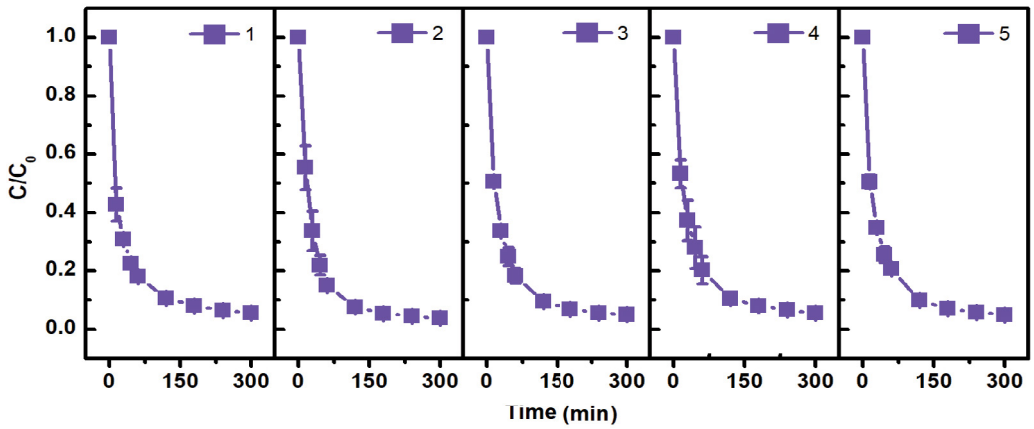

Fig. 9. ROX removal reactivity of Fe_2O_3/Mn(II) in cyclic experiments. The initial concentrations of Fe_2O_3, Mn(II) and ROX were 1.0 g L^{-1}, 0.5 mmol L^{-1} and 20.0 mg L^{-1}, respectively. The 5-run cyclic tests were carried out under the typical conditions, and Fe_2O_3 were regularly eluted by 0.1 mol L^{-1} NaOH aqueous solution. Error bars represent ± one standard deviation derived from triplicate experiments.

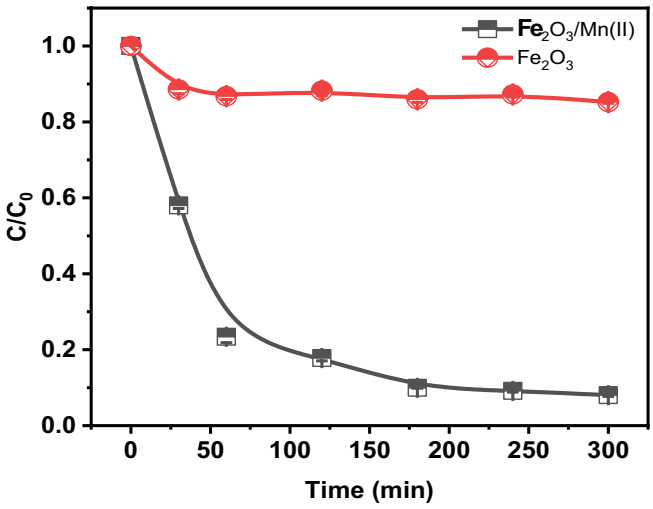

Fig. 10. Time profiles of ROX removal by Fe_2O_3 with or without Mn(II) in swine wastewater. The initial concentrations of Fe_2O_3, Mn(II) and ROX were 1.0 g L^{-1}, 0.5 mmol L^{-1} and 20.0 mg L^{-1}, respectively. Error bars represent ± one standard deviation derived from triplicate experiments.

Mn(II) could not be oxidized to Mn(III) by O_2 in the presence of Fe_2O_3, and ROX could not be oxidized. Mn(II) promoted ROX adsorption percentage from 67.16% and 88.38% within 96 h via enhancing the zeta potential of Fe_2O_3 from 5.3 to 7.5, which favored organoarsenic anions removal. These findings provide us better understanding for the migration and transformation of ROX.

Acknowledgements

This work was supported by Research Projects of Wuhan Polytechnic University (Grant 2019y12), National Natural Science Foundation of China (Grant 21906126, 21806049, 21976065). Natural Science Foundation of Hubei Province of China (2020CFB382).

References

[1] F.T. Jones, A broad view of arsenic, Poult. Sci., 86 (2007) 2–14.
[2] K.P. Mangalgiri, A. Adak, L. Blaney, Organoarsenicals in poultry litter: detection, fate, and toxicity, Environ. Int., 75 (2015) 68–80.
[3] X. Liu, W. Zhang, Y. Hu, H. Cheng, Extraction and detection of organoarsenic feed additives and common arsenic species in environmental matrices by HPLC–ICP-MS, Microchem. J., 108 (2013) 38–45.
[4] A. Sarkar, B. Paul, The global menace of arsenic and its conventional remediation – a critical review, Chemosphere, 158 (2016) 37–49.
[5] X.D. Xie, Y.N. Hu, H.F. Cheng, Mechanism, kinetics, and pathways of self-sensitized sunlight photodegradation of phenylarsonic compounds, Water Res., 96 (2016) 136–147.
[6] B.E. Hettick, J.E. Canas-Carrell, A.D. French, D.M. Klein, Arsenic: a review of the element's toxicity, plant interactions, and potential methods of remediation, J. Agric. Food Chem., 63 (2015) 7097–7107.
[7] I. Cortinas, J.A. Field, M. Kopplin, J.R. Garbarino, A.J. Gandolfi, R. Sierra-Alvarez, Anaerobic biotransformation of roxarsone and related N-substituted phenylarsonic acids, Environ. Sci. Technol., 40 (2006) 2951–2957.
[8] K.C. Makris, M. Quazi, P. Punamiya, D. Sarkar, R. Datta, Fate of arsenic in swine waste from concentrated animal feeding operations, J. Environ. Qual., 37 (2008) 1626–1633.
[9] K.E. Nachman, P.A. Baron, G. Raber, K.A. Francesconi, A. Navas-Acien, D.C. Love, Roxarsone, inorganic arsenic, and other arsenic species in chicken: a US-based market basket sample, Environ. Health Perspect., 121 (2013) 818–824.
[10] X. Xie, H. Cheng, Adsorption and desorption of phenylarsonic acid compounds on metal oxide and hydroxide, and clay minerals, Sci. Total Environ., 757 (2021) 143765, doi: 10.1016/j.scitotenv.2020.143765.
[11] A. Adamescu, W. Mitchell, I.P. Hamilton, H.A. Al-Abadleh, Insights into the surface complexation of dimethylarsinic acid on iron (oxyhydr)oxides from ATR-FTIR studies and quantum chemical calculations, Environ. Sci. Technol., 44 (2010) 7802–7807.
[12] M.J. Jimenez-Cedillo, M.T. Olguin, C. Fall, A. Colin, Adsorption capacity of iron- or iron-manganese-modified zeolite-rich tuffs for As(III) and As(V) water pollutants, Appl. Clay Sci., 54 (2011) 206–216.
[13] J.H. Kwon, L.D. Wilson, R. Sammynaiken, Sorptive uptake studies of an aryl-arsenical with iron oxide composites on an activated carbon support, Materials, 7 (2014) 1880–1898.
[14] N. Chen, Y.C. Wan, G.M. Zhan, X.B. Wang, M.Q. Li, L.Z. Zhang, Simulated solar light driven roxarsone degradation and arsenic

immobilization with hematite and oxalate, Chem. Eng. J., 384 (2020) 123254, doi: 10.1016/j.cej.2019.123254.
[15] L.Y. Wang, S.W. Wang, W.R. Chen, Roxarsone desorption from the surface of goethite by competitive anions, phosphate and hydroxide ions: significance of the presence of metal ions, Chemosphere, 152 (2016) 423–430.
[16] S.Y. Cao, X. Zhang, X.P. Huang, S.H. Wan, X.Z. An, F.L. Jia, L.Z. Zhang, Insights into the facet-dependent adsorption of phenylarsonic acid on hematite nanocrystals, Environ. Sci. Nano, 6 (2019) 3280–3291.
[17] W.R. Chen, C.H. Huang, Surface adsorption of organoarsenic roxarsone and arsanilic acid on iron and aluminum oxides, J. Hazard. Mater., 227 (2012) 378–385.
[18] A. Suda, T. Makino, Functional effects of manganese and iron oxides on the dynamics of trace elements in soils with a special focus on arsenic and cadmium: a review, Geoderma, 270 (2016) 68–75.
[19] D. Ma, J. Wu, P. Yang, M.Q. Zhu, Coupled manganese redox cycling and organic carbon degradation on mineral surfaces, Environ. Sci. Technol., 54 (2020) 8801–8810.
[20] S. Lan, X.M. Wang, Q.J. Xiang, H. Yin, W.F. Tan, G.H. Qiu, F. Liu, J. Zhang, X.H. Feng, Mechanisms of Mn(II) catalytic oxidation on ferrihydrite surfaces and the formation of manganese (oxyhydr)oxides, Geochim. Cosmochim. Acta, 211 (2017) 79–96.
[21] A.S. Madison, B.M. Tebo, A. Mucci, B. Sundby, G.W. Luther, Abundant porewater Mn(III) is a major component of the sedimentary redox system, Science, 341 (2013) 875–878.
[22] B. Chiswell, K.R. O'Halloran, Comparison of three colorimetric methods for the determination of manganese in freshwaters, Talanta, 38 (1991) 641–647.
[23] R.R. Karri, J.N. Sahu, N.S. Jayakumar, Optimal isotherm parameters for phenol adsorption from aqueous solutions onto coconut shell based activated carbon: error analysis of linear and non-linear methods, J. Taiwan Inst. Chem. Eng., 80 (2017) 472–487.
[24] Q. Hu, Y. Liu, X. Gu, Y. Zhao, Adsorption behavior and mechanism of different arsenic species on mesoporous $MnFe_2O_4$ magnetic nanoparticles, Chemosphere, 181 (2017) 328–336.
[25] Y. Zhu, X. Wang, J. Zhang, L. Ding, J. Li, H. Zheng, C. Zhao, Generation of active Mn(III)aq by a novel heterogeneous electro-permanganate process with manganese(II) as promoter and stabilizer, Environ. Sci. Technol., 53 (2019) 9063–9072.
[26] M. Ding, B. de Jong, S.J. Roosendaal, A. Vredenberg, XPS studies on the electronic structure of bonding between solid and solutes: adsorption of arsenate, chromate, phosphate, Pb^{2+}, and Zn^{2+} ions on amorphous black ferric oxyhydroxide, Geochim. Cosmochim. Acta, 64 (2000) 1209–1219.
[27] B. Li, D. Wei, Z. Li, Y. Zhou, Y. Li, C. Huang, J. Long, H. Huang, B. Tie, M. Lei, Mechanistic insights into the enhanced removal of roxsarsone and its metabolites by a sludge-based, biochar supported zerovalent iron nanocomposite: adsorption and redox transformation, J. Hazard. Mater., 389 (2020) 122091, doi: 10.1016/j.jhazmat.2020.122091.
[28] C. Chen, L. Liu, Y. Li, L. Zhou, Y. Lan, Efficient degradation of roxarsone and simultaneous in-situ adsorption of secondary inorganic arsenic by a combination of Co_3O_4-Y_2O_3 and peroxymonosulfate, J. Hazard. Mater., 407 (2021) 124559, doi: 10.1016/j.jhazmat.2020.124559.
[29] M. Chabot, T. Hoang, H.A. Al-Abadleh, ATR-FTIR studies on the nature of surface complexes and desorption efficiency of p-arsanilic acid on iron (oxyhydr)oxides, Environ. Sci. Technol., 43 (2009) 3142–3147.
[30] W. Zhao, H. Cheng, S. Tao, Structure-reactivity relationships in the adsorption and degradation of substituted phenylarsonic acids on birnessite (δ-MnO_2), Environ. Sci. Technol., 54 (2020) 1475–1483.
[31] C.Ó. Nualláin, S.Ó. Cinnéide, The thermodynamic ionization constants of aromatic arsonic acids, J. Inorg. Nucl. Chem., 35 (1973) 2871–2881.
[32] Q. Liu, X. Lu, H. Peng, A. Popowich, J. Tao, J.S. Uppal, X. Yan, D. Boe, X.C. Le, Speciation of arsenic – a review of phenyl-arsenicals and related arsenic metabolites, TrAC, Trends Anal. Chem., 104 (2018) 171–182.